

## **The impact of increasing carbon dioxide on ozone recovery**

Joan E. Rosenfield<sup>1</sup>  
University of Maryland Baltimore County, Baltimore, Maryland

Anne R. Douglass  
NASA Goddard Space Flight Center, Greenbelt, Maryland

David B. Considine  
University of Maryland, College Park, Maryland

**Abstract.**

We have used the GSFC coupled two-dimensional (2D) model to study the impact of increasing carbon dioxide from 1980 to 2050 on the recovery of ozone to its pre-1980 amounts. We find that the changes in temperature and circulation arising from increasing CO<sub>2</sub> affect ozone recovery in a manner which varies greatly with latitude, altitude, and time of year. Middle and upper stratospheric ozone recovers faster at all latitudes due to a slowing of the ozone catalytic loss cycles. In the lower stratosphere, the recovery of tropical ozone is delayed due to a decrease in production and a speed up in the overturning circulation. The recovery of high northern latitude lower stratospheric ozone is delayed in spring and summer due to an increase in springtime heterogeneous chemical loss, and is speeded up in fall and winter due to increased downwelling. The net effect on the higher northern latitude column ozone is to slow down the recovery from late March to late July, while making it faster at other times. In the high southern latitudes, the impact of CO<sub>2</sub> cooling is negligible. Annual mean column ozone is predicted to recover faster at all latitudes, and globally averaged ozone is predicted to recover approximately ten years faster as a result of increasing CO<sub>2</sub>.

## 1. Introduction

As the halogen loading of the stratosphere decreases, ozone is expected to recover to its pre-1980 values in about 2050 (WMO, 1999). A topic of much concern is the effect that increases in the greenhouse gas CO<sub>2</sub> will have on this recovery. Modeling studies have generally agreed that increases in CO<sub>2</sub> will lead to a cooling of the stratosphere (e.g. Fels *et al.*, 1980; Rind *et al.*, 1990). This cooling is expected to reduce temperature dependent loss processes, resulting in increases in upper stratospheric ozone (e.g. Brasseur and Hitchman, 1988; Pitari *et al.*, 1992). Recently, some studies using a three-dimensional (3D) model and a highly parameterized chemistry scheme have indicated that the stratospheric cooling due to the build-up of greenhouse gases would lead to increases in polar stratospheric clouds (PSCs) resulting in larger seasonal ozone depletions [Shindell *et al.*, 1998a; Shindell *et al.*, 1998b]. Their proposed mechanism is a reduction of planetary wave propagation into the stratosphere, resulting in a polar cooling. These authors suggest that ozone recovery will be slower than expected solely from the projected decline in stratospheric chlorine loading. A series of one-year simulations by a general circulation model with coupled chemistry [Austin *et al.*, 2000] were carried out for six years during the 1979 to 2014 time period. The results suggested that increasing greenhouse gases were delaying the onset of ozone recovery. A survey of transient chemistry-climate experiments using four different 3D models was summarized in WMO 1999. Three of the models showed increasing Arctic losses as a result of increasing CO<sub>2</sub>, while one model showed no significant changes. Of these 3D models, however, those having full chemistry schemes were limited to runs of less than a decade. Those 3D models capable of runs several decades long had highly simplified chemistry schemes. Because of computational costs, long runs with interactive full chemistry and radiation are currently limited to two-dimensional (2D) models.

We have used the GSFC coupled two-dimensional (2D) model to study the impact of increasing carbon dioxide from 1980 to 2050 on the stratospheric recovery of ozone to its pre-1980 values. The residual circulation in the coupled model changes in response to both radiative forcing changes and changes in the planetary wave propagation computed with a planetary wave parameterization. However, tropospheric wave forcing is fixed. It is unclear how changes in tropospheric wave forcing would alter the stratospheric circulation, and 3D models have obtained inconsistent results on this issue [Mahfouf *et al.*, 1994; Butchart *et al.*, 2000; Rind *et al.*, 1990]. Thus we will focus primarily on the interactions between radiation and chemistry, in a manner complementary to other studies of this problem [e.g., Shindell *et al.*, 1998]. In Section 2 we summarize the relevant model characteristics, in Section 3 we present the results, and in Section 4 we give the summary and conclusions.

## 2. Model

The Goddard coupled 2D (latitude-pressure) chemistry-radiation-dynamics model is fully interactive in temperature, ozone, and water vapor. The model has full chemistry and radiation schemes and has been described in Rosenfield *et al.* [1997], with improvements given in Rosenfield *et al.* [1998] and Rosenfield and Douglass [1998]. These improvements include the use of model generated water vapor, as well as ozone and temperatures, in the radiative heating calculation, the radiative heating due to PSCs, and the use of the Lin and Rood [1996] scheme for the numerical advection of atmospheric trace species. Gases included in the radiation calculation are carbon dioxide, ozone, and water vapor. Advection in the dynamics module uses the Prather second-order moments transport scheme [Prather, 1986]. The chemical reaction rates and photolysis cross sections used are those given in the Jet Propulsion Laboratory (JPL) recommendation [DeMore *et al.*, 1997].

The model dynamics incorporates a planetary wave parameterization which propagates waves, calculates the wave-mean flow interaction, and estimates the meridional eddy diffusivity produced by wave dissipation [Bacmeister *et al.*, 1995]. The planetary waves are forced from below by topography. Thus, although there is no interannual variability in tropospheric wave forcing, the stratospheric wave propagation and eddy mixing can respond to temperature changes induced by increasing CO<sub>2</sub>.

The model chemistry includes a detailed treatment of heterogeneous chemistry on background stratospheric aerosol and polar stratospheric clouds. The condensed mass of PSCs is calculated by integrating over an observationally based temperature probability distribution which takes into account the longitudinal variations in temperature, as described in Considine *et al.* [1994] and Rosenfield *et al.* [1997]. In this work the probability distribution has been shifted to colder temperatures by 2 K, to be consistent with the present day observed Arctic ozone losses. Particle sedimentation is included, but the effects of volcanic aerosols have not been included in this study.

Time dependent runs used natural and anthropogenic source gas boundary conditions given by Scenario A3 of WMO 1999. These correspond to the maximum emissions allowed within protocols. Surface chlorine loadings were 2.4 ppbv in 1980, increasing to 3.6 ppbv in 1995, and declining thereafter. The model was run from 1970 through 2050, the years 1970 to 1980 being allowed for spin-up. CO<sub>2</sub> mixing ratios increase from 325 ppmv in 1980 to 509 ppmv in 2050. Another run was done in which all source gas boundary conditions changed with time except for CO<sub>2</sub>, which was fixed at its 1980 value.

### 3. Results

#### a. Global column ozone

Figure 1 shows modeled 1990 column ozone as a function of latitude and day of year (Fig. 1a) compared with TOMS (Fig. 1b). The high latitude maximum is on the pole in the northern hemisphere (NH) and off the pole in the southern hemisphere (SH), in agreement with observations. Column ozone amounts are within about 10% of TOMS (Fig. 1c) except in the high southern latitudes. The Antarctic springtime ozone hole occurs about one month later than observed. This may be due to the fact that the model cannot account for excursions of the vortex off the pole. The return of the Antarctic column ozone to pre-springtime values is slower in the model than in observations. This is likely due to insufficient high latitude meridional mixing at the time of vortex breakup.

Figure 2 shows the differences from 1980 of annually, globally averaged column ozone amounts for the increasing and fixed  $\text{CO}_2$  simulations. For both simulations minimum ozone amounts are reached in 1998, followed by a recovery which is slower for the fixed  $\text{CO}_2$  case. Increasing  $\text{CO}_2$  is seen to speed up the recovery to 1980 values by approximately ten years, with the fixed  $\text{CO}_2$  ozone recovering in the year 2046 and the increasing  $\text{CO}_2$  ozone recovering in the year 2037.

Figure 3 shows the year of recovery of column ozone to 1980 values as a function of day of year and latitude. Increasing  $\text{CO}_2$  speeds up the recovery of column ozone in all seasons in the low and middle latitudes. Recovery is fastest in the tropics, with a speedup due to increasing  $\text{CO}_2$  of between 5 and 10 years. In the middle latitudes, the speedup in recovery with increasing  $\text{CO}_2$  is greatest in the fall and winter months. In the polar latitudes, increasing  $\text{CO}_2$  speeds up NH recovery in the fall and winter and slows it down in spring and early summer, and speeds up SH recovery in the fall and winter. Annual mean column ozone recovers faster at all latitudes (not shown). We present the results in more detail in the following two sub-sections.

## b. Tropics

As seen in Figure 3, the computed effect of increasing CO<sub>2</sub> on low latitude column ozone recovery shows relatively little seasonal variability. We therefore focus on the annual mean results. Figure 4 shows annual mean ozone mixing ratio differences from 1980 at 5N as a function of year and pressure. There is a faster recovery with increasing CO<sub>2</sub> above about 30 hPa. Below 30 hPa there is no recovery out to year 2050 in the increasing CO<sub>2</sub> case. The net effect on the column ozone amount is a faster recovery.

To understand the differing behavior with altitude, we need to examine the changes in temperature, vertical velocity, and ozone chemical production and loss. Figure 5 shows annual mean temperature differences from 1980 as a function of year and pressure at 5N. With fixed CO<sub>2</sub>, reductions in upper stratospheric temperatures on the order of 0.5 - 1 K are computed. This cooling is due to decreased solar heating as a result of ozone losses. With increasing CO<sub>2</sub>, an increase in infrared cooling leads to a cooling of the stratosphere. Upper stratospheric temperatures drop by more than 5 K by the year 2050. The upper troposphere is computed to warm by less than 1 K. The feedback of the computed ozone changes on the heating rates results in smaller absolute temperature changes than would be computed without this feedback.

Vertical velocity differences between the varying CO<sub>2</sub> run and the fixed CO<sub>2</sub> run at 5N are shown in Figure 6. As has been shown before in a doubled CO<sub>2</sub> experiment, increasing CO<sub>2</sub> will increase the residual circulation in the middle and upper stratosphere (e.g., *Rosenfield and Douglass, 1998*). In this study the increase in tropical upper stratospheric vertical velocities reaches a maximum of 5% in the year 2050. In the lower stratosphere the increasing CO<sub>2</sub> leads to a 2-3% increase in vertical velocity maximizing at 70 hPa after the year 2010. Lower temperatures increase the modeled infrared heating which is greater than the solar heating in 16-18 km region.

The computed chemical loss frequencies for the various gas phase catalytic destruction cycles are shown in Figure 7 for the year 1980. Figure 8 shows the change of 2020 loss frequencies from 1980, with and without changing CO<sub>2</sub>. Throughout most of the stratosphere the cooling due to increasing CO<sub>2</sub>

leads to a reduction in the loss frequencies for each of the cycles. These reductions can be attributed to both a direct effect and indirect effects of cooling. A direct effect of cooling is the well known slowing of the ozone recombination reaction  $O + O_3 \rightarrow 2 O_2$ , whose rate constant is proportional to  $\exp(-2060/T)$ . This explains the reduction of the loss frequency due to the Ox cycle. The rate determining steps of the remaining loss cycles do not have a large temperature dependence.

Indirect effects of cooling are a decrease in NOy and a decrease in the O/Ox ratio. Computed changes in upper stratospheric NOy and the O/Ox ratio for the 1980 to 2050 period are shown in Figure 9. NOy is increasing with time because of the increasing abundance of the greenhouse gas N<sub>2</sub>O. However, the increase in NOy is less when one takes into account the cooling due to CO<sub>2</sub> increases. A reduction in NOy with cooling has been shown [Rosenfield and Douglass, 1998] to arise from the very large temperature dependence of the reaction  $N + O_2 \rightarrow NO + O$  ( $k \sim \exp(3600/T)$ ). The abundance of N is increased with cooling, leading to an increase in the loss of NOy which is controlled by the reaction  $N + NO \rightarrow N_2 + O$ . This decrease in NOy contributes to the reduction of the ozone loss frequency due to the NOx cycle.

The O/Ox ratio changes very little with time when CO<sub>2</sub> is fixed, while decreasing markedly when CO<sub>2</sub> cooling occurs. This decrease with cooling of the O/Ox ratio results from a change in the O/O<sub>3</sub> partitioning, which is controlled by the reaction  $O + O_2 + M \rightarrow O_3 + M$ . The rate constant for this reaction is proportional to  $[300/T]^{2.3}$ . This decrease of O/Ox contributes to the slowing of all the ozone catalytic loss cycles with cooling. Since NO<sub>x</sub> dominates at 30-2 hPa, a slowdown of NO<sub>x</sub> loss has the largest impact.

In the middle and upper stratosphere, the chemical loss term dominates the transport term in the ozone tendency equation. We can thus attribute the faster recovery of tropical ozone mixing ratios above ~30 hPa to the slowing of the chemical loss cycles with cooling. While ozone increases in the tropical middle and upper stratosphere have been noted before as a result of increasing CO<sub>2</sub> [e.g. Rind *et al.*, 1998], we have shown using our detailed chemistry scheme that these increases are attributable to a combination of changes in both NOy amounts and partitioning within the Ox species. In the tropical

lower stratosphere the ozone loss is dominated by the HOx catalytic cycle, which shows a small change with cooling which changes sign at 70 hPa. Lower stratospheric ozone production, however, is computed to be reduced by roughly 2% due to the effects of the middle and upper stratospheric ozone increases on O<sub>2</sub> photolysis rates. This is the reverse of "self-healing", an increase in lower stratospheric tropical ozone calculated as a result of upper stratospheric losses due to increased chlorine [Hudson, 1977, p.201]. We thus attribute the delayed recovery of lower stratospheric ozone to the combined effects of decreased production and increased upwelling. The middle and upper stratospheric changes outweigh those of the lower stratosphere, leading to a faster recovery of the column.

### **c. Extra-tropics**

At high latitudes, lower stratospheric cooling is expected to cause increases in PSCs and a potential enhancement of springtime ozone destruction. Figure 10 (top) shows the computed annual mean column ozone differences from 1980 as a function of year at 75N and 75S, for the increasing CO<sub>2</sub> case. The maximum depletions relative to 1980 occur during the years 1998-2000. Figure 10 (bottom) shows the 1998-2000 mean column ozone differences, relative to 1980, at 75N and 75S as a function of day of year. Maximum springtime depletions of ~42% and ~12% are computed in October at 75S and in April at 75N, respectively. Observations show that the lowest ozone values occur about one month earlier than computed, in March and September for the NH and SH, respectively. We have seen in Figure 1 that the Antarctic ozone hole occurs later in the model than observations. As a comparison, TOMS 70-80N zonal mean differences for the March 1998-2000 average relative to the March 1979-1980 average are -9.4%. The corresponding TOMS differences at 70-80S in September are -40%.

A major contributor to the springtime column ozone losses are lower stratospheric decreases of ~20-25% in the NH and 90-100% in the SH (not shown). These losses are due to the activation of chlorine as a result of heterogeneous reactions occurring on the surfaces of PSCs. As mentioned in Section 2, the temperature probability distribution used in the computation of PSC amounts was shifted to slightly colder temperatures to ensure the approximate agreement of computed with observed present day

ozone depletions. At the onset of spring, computed lower stratospheric chlorine activation is roughly 30-40% at 75N and close to 100% at 75S.

Associated with the computed chlorine activation is denitrification. At 75S, model computed NO<sub>y</sub> in the 1998-2000 winter is ~90% less than that computed in a run with no heterogeneous chemistry. Moderate denitrification of ~30-40% is computed at 75N. Evidence for moderate Arctic denitrification has been observed in years with cold stable Arctic vortices [*Rex et al.*, 1999; *Santee et al.*, 2000; *Fahey et al.*, 2001].

We turn now to the effects of increasing CO<sub>2</sub> on the recovery of high latitude ozone. As shown in Figure 3, the effect of changing CO<sub>2</sub> on column ozone in the high northern latitudes depends on the time of year. Column ozone recovers to its 1980 values slower from late March to late July while recovering faster the rest of the year. In the annual mean the column recovery is faster with increasing CO<sub>2</sub>. Figure 11 shows the annual mean ozone profile differences from 1980 at 75N. Above about 50 hPa, where approximately 43% of the total column resides, the recovery is faster with increasing CO<sub>2</sub>, while below it is slower. The faster recovery above 50 hPa occurs throughout the year, and the same reasons hold as did for the tropical upper stratosphere - i.e. the lowered NO<sub>y</sub> and O/O<sub>x</sub> due to colder temperatures slow the gas phase ozone destruction reactions.

The slower recovery of ozone in the high northern latitude lower stratosphere is a result of increasing springtime heterogeneous loss. Figure 12a shows computed ozone mixing ratios throughout the year 2020 at 75N and 68 hPa. Ozone amounts start declining from their late winter high values in March, reaching their lowest values in late August, after which downwelling brings down air containing higher ozone amounts.

With increasing CO<sub>2</sub> there is a faster decline in March and April, and a slower decline from May through August (Fig. 12b). During March and April between ~40-70 hPa there is a 20-35% increase in the chlorine catalyzed loss arising from increased heterogeneous processing. A 1-2 K cooling leads to an increased amount of PSCs and denitrification. For example, maximum amounts of Type I PSCs at 68 hPa in the year 2020 increase 43%, and late winter to early spring denitrification increases from 35% to

about 45% with cooling. Computed Type II PSCs are negligible in the high northern latitudes. Although HCl mixing ratios are very small in both cases due to the  $\text{HCl} + \text{ClONO}_2 \rightarrow \text{Cl}_2 + \text{HNO}_3$  reaction, the increase in surface area and the colder temperatures allow the  $\text{ClONO}_2 + \text{H}_2\text{O} \rightarrow \text{HOCl} + \text{HNO}_3$  reaction to be more important. This explains the greater spring ozone loss due to the chlorine catalytic cycle. After April, ozone loss is controlled by the gas phase processes. From late spring through summer the net ozone loss frequency is less for the increasing  $\text{CO}_2$  case, mainly due to a reduction in the  $\text{NO}_x$  cycle as a result of lower  $\text{NO}_y$ . In fall and winter an increase in downwelling in the changing  $\text{CO}_2$  case results in higher values of ozone.

Figure 13 shows ozone differences from 1980 at 75N and 68 hPa as a function of year and month. After springtime ozone reaches its lowest levels in approximately the year 2000, the beginnings of recovery occur roughly ten years later in the increasing  $\text{CO}_2$  case. At this level the ozone recovery to its 1980 values is slowed down between March and October and speeded up at other times.

In the southern high latitudes, computed column ozone recovers faster throughout the year with increasing  $\text{CO}_2$  (not shown). In the middle and upper stratosphere the faster recovery is due to the reduction in  $\text{NO}_y$  and  $\text{O/O}_x$ , which slows down the gas phase loss reactions. In the lower stratosphere, ozone has a faster recovery during fall and winter months due to increased downwelling. The impact on springtime lower stratospheric ozone depletion is negligible. Although additional cooling results in the formation of higher amounts of Type I PSC, chlorine activation is already nearly complete and ozone loss nearly 100% in the fixed  $\text{CO}_2$  case.

The planetary wave parameterization included in the model formulation allows for the computation of horizontal eddy mixing. This results in some mixing of the high latitude springtime ozone depletions into the middle latitudes, thus slowing the northern middle latitude ozone recovery below about 40 hPa for some seasons. For example, at 45N and 68 hPa, increasing  $\text{CO}_2$  causes ozone recovery to be slowed down from April to October. The middle and upper stratospheric speed up in ozone recovery dominates, resulting in a faster recovery of column ozone in the middle latitudes.

#### 4. Summary and Conclusions

Our 2D coupled model results show that both direct and indirect feedbacks affect the global distribution of ozone. The changes in temperature and circulation arising from increasing CO<sub>2</sub> affect ozone recovery in a manner which varies greatly with latitude, altitude, and time of year. Firstly, the stratospheric cooling due to increasing CO<sub>2</sub> feeds back on the temperature dependent homogeneous reaction rates. This affects ozone loss rates both directly and indirectly, resulting in a slowing of all the ozone catalytic loss cycles in the middle and upper stratosphere. Ozone is predicted to recover to 1980 values faster throughout the year above ~30 hPa in the tropics and above ~50 hPa in the extra-tropics, with increasing CO<sub>2</sub>. Secondly, in the tropics below ~30 hPa, ozone recovery is predicted to be slowed down by both a decrease in production and an increase in upwelling.

In the high latitude northern lower stratosphere, ozone recovery is predicted to be slowed down in spring and summer due to an increase in springtime heterogeneous chemical loss due to the CO<sub>2</sub> cooling. Some of this increased high northern latitude chemical loss is mixed into the middle latitudes. In the high southern latitudes, the impact of CO<sub>2</sub> cooling is negligible. High latitude lower stratospheric ozone recovery is predicted to be hastened in the fall and winter by an increase in downwelling.

In the annual mean, column ozone is predicted to recover faster at all latitudes with increasing CO<sub>2</sub>. In the tropics the column ozone recovers faster in all seasons, while in the high northern latitudes, column ozone recovery is slowed down from late March to late July and speeded up the rest of the year. In the global mean, the increasing high northern latitude ozone depletion caused by the increase in PSCs calculated in a cooler lower stratosphere is outweighed by ozone increases at higher altitudes and lower latitudes. As a result, the model results suggest that increasing CO<sub>2</sub> will hasten the recovery of globally averaged column ozone by approximately ten years.

The model planetary wave scheme includes the effects of dynamical changes in the stratospheric planetary wave propagation. *Shindell et al.* [1996a] noted that the refraction of planetary waves into the tropics as a result of greenhouse gas cooling reduced the frequency of stratospheric warmings and exacerbated polar cooling. Our model includes these processes in a parameterized way, but we find the

changes in wave propagation to be negligible. We note that 3D models do not agree on this point [Mahfouf *et al.*, 1994; Butchart *et al.*, 2000]. Much colder lower stratospheric temperatures, whether caused by dynamical changes which we cannot model in a 2D framework or other causes, would result in an increase in NH high latitude heterogeneous processing. The effect on ozone recovery in the middle latitudes and thus globally averaged ozone recovery would depend on the extent to which the high latitude depletions mix to lower latitudes. In the absence of significant changes in tropospheric wave forcing, a purely radiative cooling of the stratosphere due to increasing CO<sub>2</sub> leads to a faster recovery of the global average ozone.

**Acknowledgments.** We thank Paul Newman, Julio Bacmeister, Mark Schoeberl, and Rich Stolarski for helpful comments.

<sup>1</sup>Mailing address: Code 916, NASA Goddard Space Flight Center, Greenbelt, MD 20771  
(rose@euterpe.gsfc.nasa.gov)

## References

- Angell, J. K., Difference in radiosonde temperature trend for the period 1979-1998 of MSU data and the period 1959-1998 twice as long, *Geophys. Res. Lett.*, *27*, 2177-2180, 2000.
- Austin, J., J. Knight, and N. Butchart, Three-dimensional chemical model simulations of the ozone layer: 1979-2015, *Q. J. R. Meteorol. Soc.*, *126*, 1533-1556, 2000.
- Bacmeister, J.T., M.R. Schoeberl, M.E. Summers, J.E. Rosenfield, and X. Zhu, Descent of long-lived trace gases in the winter polar vortex, *J. Geophys. Res.*, *100*, 11,669-11,684, 1995.
- Brasseur, G., and M. Hitchman, Stratospheric response to trace gas perturbations - changes in ozone and temperature distributions, *Science*, *240*, 634-637, 1988.
- Butchart, N., J. Austin, J.R. Knight, A.A. Scaife, and M.L. Gallani, The response of the stratospheric climate to projected changes in the concentrations of well-mixed greenhouse gases from 1992 to 2051, *J. Climate*, *13*, 2142-2159, 2000.
- DeMore, W. B., Chemical kinetics and photochemical data for use in stratospheric modeling, Evaluation number 12, *JPL Publ.*, *97-4*, 266 pp., 1997.
- Fahey, D.W., et al., The detection of large HNO<sub>3</sub>-containing particles in the winter arctic stratosphere, *Science*, *291*, 1026-1031, 2001.
- Fels, S.B., J.D. Mahlman, M.D. Schwarzkopf, and R.W. Sinclair, Stratospheric sensitivity to perturbations in ozone and carbon dioxide: radiative and dynamical response, *J. Atmos. Sci.*, *37*, 2256-2297, 1980.
- Hudson, R.D. (Ed.), Chlorofluoromethanes and the stratosphere, *NASA Ref. Publ. 1010*, 266 pp., 1977.
- Lin, S.-J., and R.B. Rood, Multidimensional flux-form semi-Lagrangian transport schemes, *Mon. Weather Rev.*, *124*, 2046-2070, 1996.
- Mahfouf, J.F., D. Cariolle, J.-F. Royer, J.-F. Geleyn, and B. Timal, Response of the Meteo-France climate model to changes in CO<sub>2</sub> and sea surface temperature, *Clim. Dyn.*, *9*, 345-362, 1994.
- Pawson, S., K. Labitzke, and S. Leder, Stepwise changes in stratospheric temperature, *Geophys. Res. Lett.*, *25*, 2157-2160, 1998.
- Pawson, S., and B. Naujokat, The cold winters of the middle 1990s in the northern lower stratosphere, *J.*

*Geophys. Res.*, 104, 14,209-14,222, 1999.

Pitari, G., S. Palmeri, and G. Visconti, Ozone response to a CO<sub>2</sub> doubling: Results from a stratospheric circulation model with heterogeneous chemistry, *J. Geophys. Res.*, 97, 5953-5962, 1992.

Prather, M.J., Numerical advection by conservation of second-order moments, *J. Geophys. Res.*, 91, 6671-6681, 1986.

Rex, M., et al., Subsidence, mixing, and denitrification of Arctic polar vortex air measured during POLARIS, *J. Geophys. Res.*, 104, 26,611-26,623, 1999.

Rind, D., R. Suozzo, N.K. Balachandran, and M.J. Prather, Climate change and the middle atmosphere. Part I: The doubled CO<sub>2</sub> climate, *J. Atmos. Sci.*, 47, 475-494, 1990.

Rind, D., D. Shindell, P. Lonergan, N.K. Balachandran, Climate change and the middle atmosphere. Part III: The doubled CO<sub>2</sub> climate revisited, *J. Climate*, 11, 876-894.

Rosenfield, J. E., et al., Stratospheric effects of Mount Pinatubo aerosol studied with a coupled two-dimensional model, *J. Geophys. Res.*, 102, 3649-3670, 1997.

Rosenfield, J. E., et al., The impact of subvisible cirrus clouds near the tropical tropopause on stratospheric water vapor, *Geophys. Res. Lett.*, 25, 1883-1886, 1998.

Rosenfield, J. E. and A. R. Douglass, Effects on NO<sub>y</sub> in a coupled 2D model, *Geophys. Res. Lett.*, 25, 4381-4384, 1998.

Santee, M. L., G. L. Manney, N. J. Livesey, and J. W. Waters, UARS Microwave Limb Sounder observations of denitrification and ozone loss in the 2000 arctic late winter, *Geophys. Res. Lett.*, 27, 3213-3216, 2000.

Shindell, D.T., D. Rind, and P. Lonergan, Increased polar stratospheric ozone losses and delayed eventual recovery owing to increasing greenhouse-gas concentrations, *Nature* 392, 589-592, 1998a.

Shindell, D.T., D. Rind, and P. Lonergan, Climate change and the middle atmosphere. Part IV: ozone response to doubled CO<sub>2</sub>, *J. of Clim.*, 11, 895-918, 1998b.

WMO, Scientific Assessment of Ozone Depletion: 1998, Rep. No. 44, Geneva, 1999.

## FIGURE CAPTIONS

Figure 1. (a) Computed column ozone (DU) in 1990 as a function of day of year and latitude. (b) TOMS column ozone (DU) averaged for the years 1988-1992 as a function of day of year and latitude. (c) Percent difference of computed from TOMS column ozone. The model year has 360 days.

Figure 2. Time series of percent difference of annually, globally averaged ozone from 1980. Solid line is increasing CO<sub>2</sub> case, and dashed line is fixed CO<sub>2</sub> case.

Figure 3. (top) Year of column ozone recovery to 1980 values as a function of day of year and latitude for fixed CO<sub>2</sub> case. (bottom) Same as top except for increasing CO<sub>2</sub> case. The model year has 360 days.

Figure 4. Computed percent differences of annual mean ozone mixing ratios from 1980 values at 5N with (top) CO<sub>2</sub> fixed at 1980 values and (bottom) CO<sub>2</sub> increasing.

Figure 5. Computed annual mean temperature differences from 1980 at 5N with (top) CO<sub>2</sub> fixed at 1980 values and (bottom) CO<sub>2</sub> increasing.

Figure 6. Computed percent differences of annual mean vertical velocities at 5N for the increasing CO<sub>2</sub> case compared with the fixed CO<sub>2</sub> case.

Figure 7. Computed 1980 annual mean Ox loss frequencies at 5N.

Figure 8. Computed percent differences of annual mean Ox loss frequencies (2020 - 1980) at 5N. Solid lines refer to increasing CO<sub>2</sub>, while dashed lines refer to fixed 1980 CO<sub>2</sub>.

Figure 9. Percent changes of annual mean NO<sub>y</sub> and O/Ox at 5N and 3 hPa. Solid lines refer to the increasing CO<sub>2</sub> case, while dashed lines refer to fixed CO<sub>2</sub> case.

Figure 10. (a) Computed percent difference of annual mean column ozone from 1980 at 75S (solid) and 75N (dashed), for the case of increasing CO<sub>2</sub>; (b) computed percent difference of 1998-2000 mean column ozone from 1980 at 75N (dashed) and 75S (solid), for the case of increasing CO<sub>2</sub>.

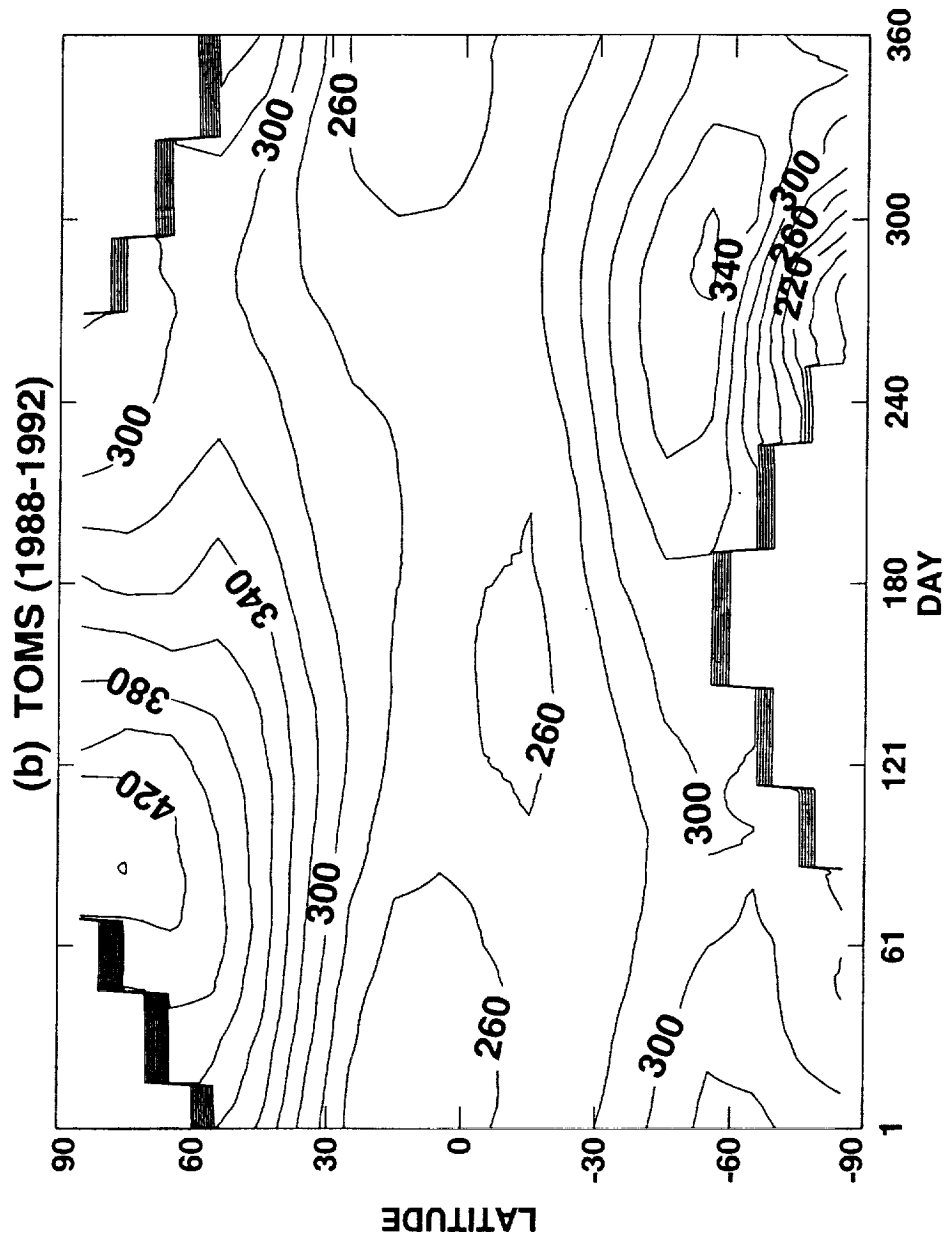
Figure 11. Computed percent differences of annual mean ozone mixing ratios from 1980 values at 75N with (top) CO<sub>2</sub> fixed at 1980 values and (bottom) CO<sub>2</sub> increasing.

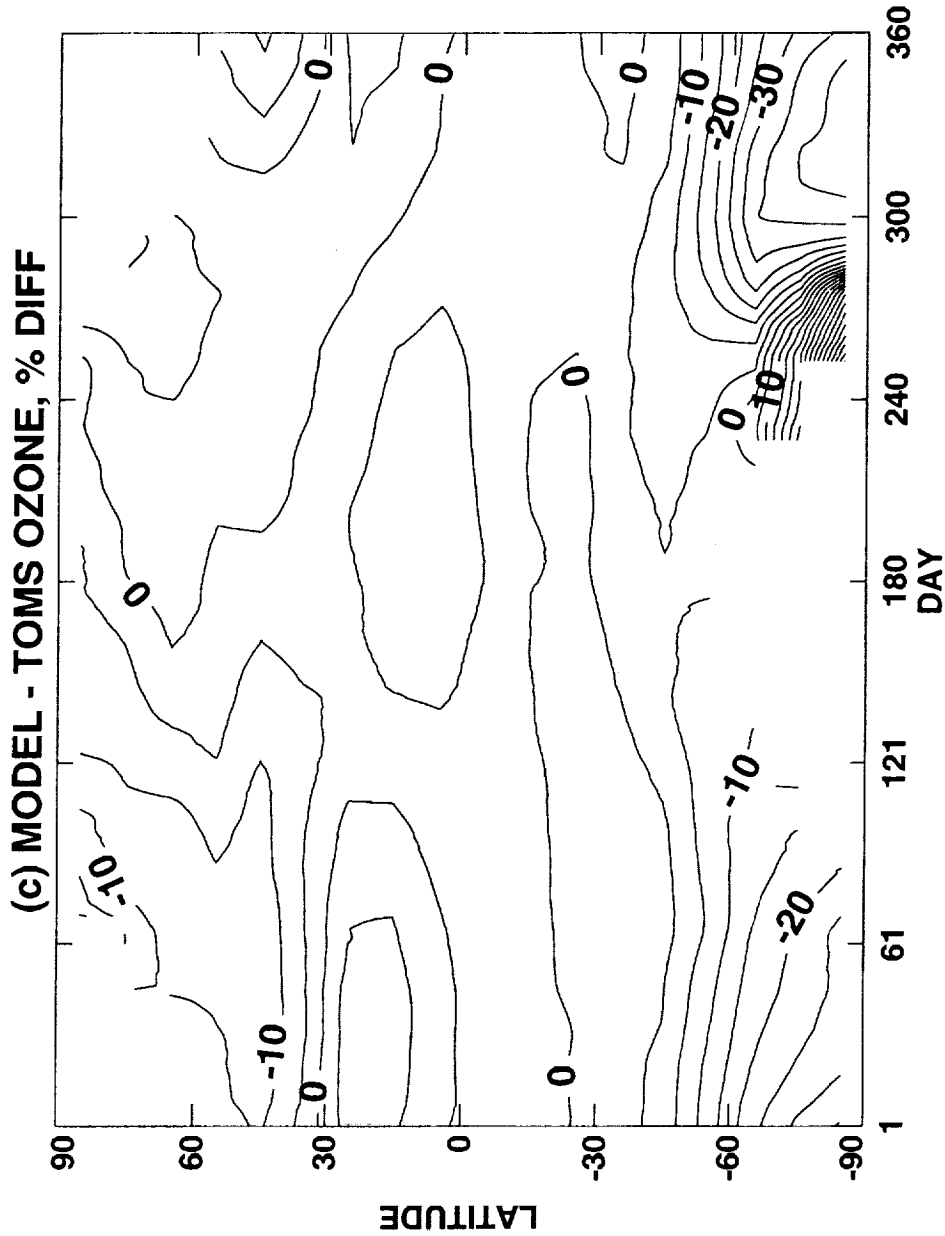
Figure 12. (a) Computed ozone mixing ratios in the year 2020 at 75N and 67 hPa for increasing CO<sub>2</sub>

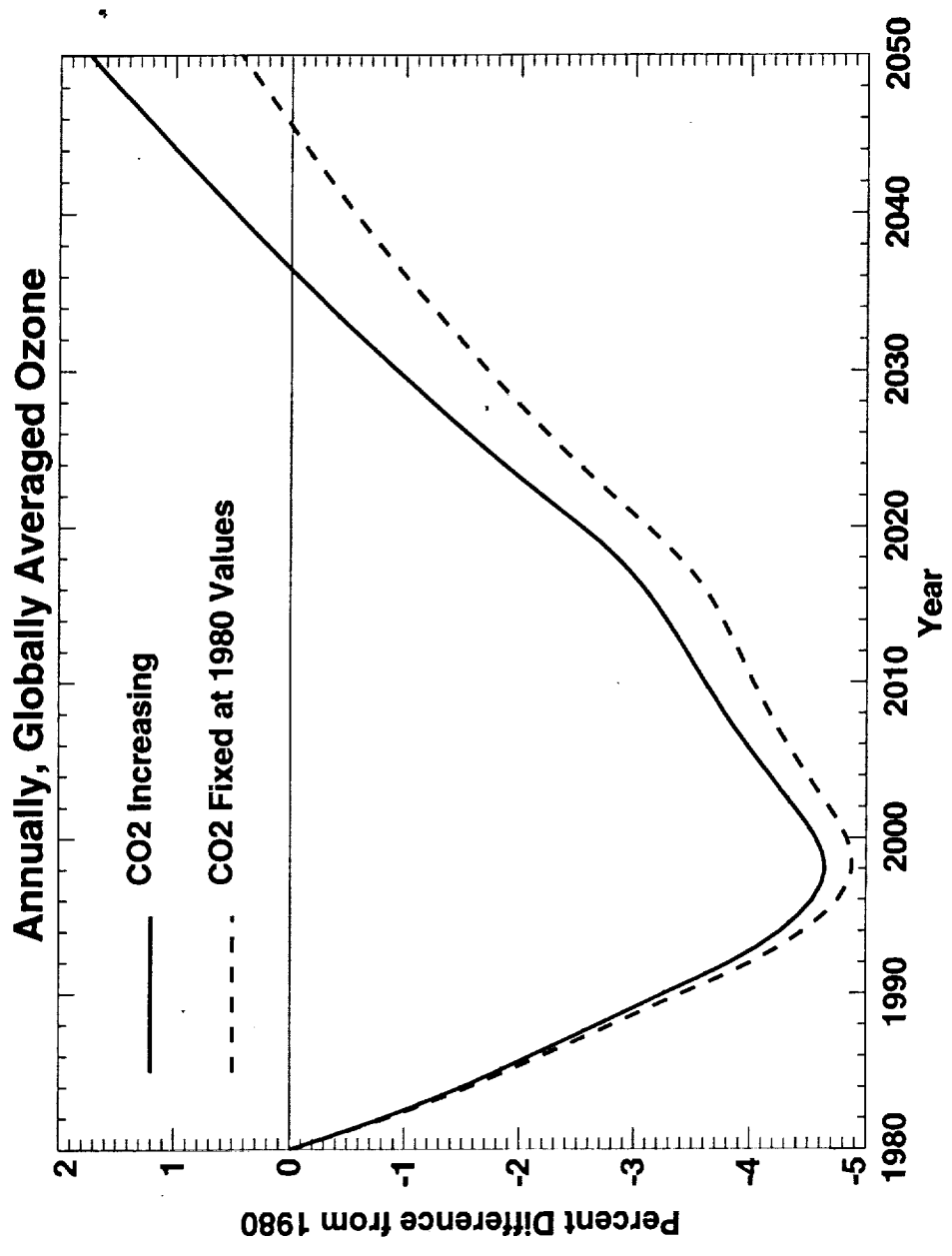
(solid) and fixed 1980 CO<sub>2</sub> (dashed). Tick marks are at the middle of the months. (b) Difference of ozone mixing ratios in 2020 at 75 N and 67 hPa (increasing CO<sub>2</sub> minus fixed CO<sub>2</sub> case).

Figure 13. Computed percent differences of ozone mixing ratios at 75N and 67 hPa from 1980 values with (top) CO<sub>2</sub> fixed at 1980 values and (bottom) CO<sub>2</sub> increasing.

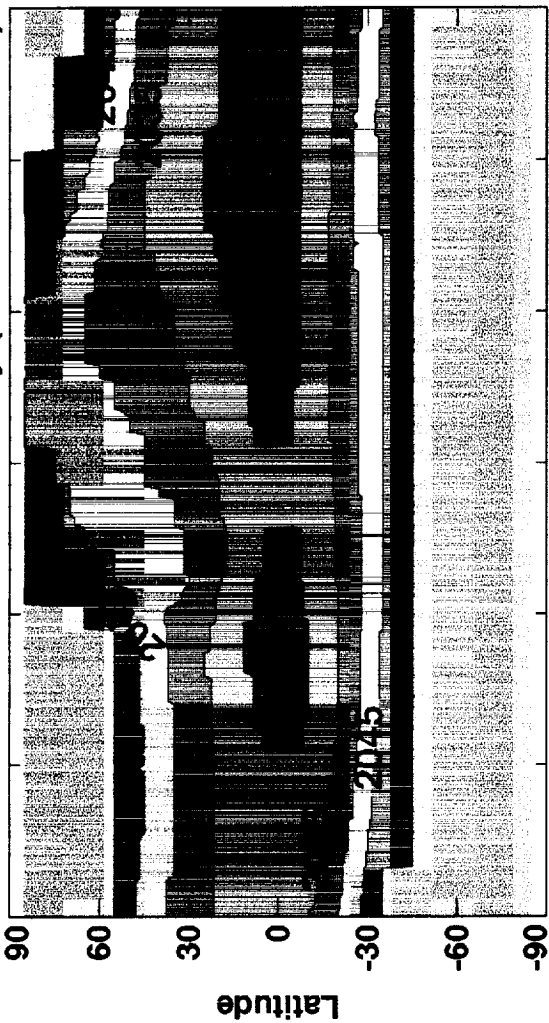






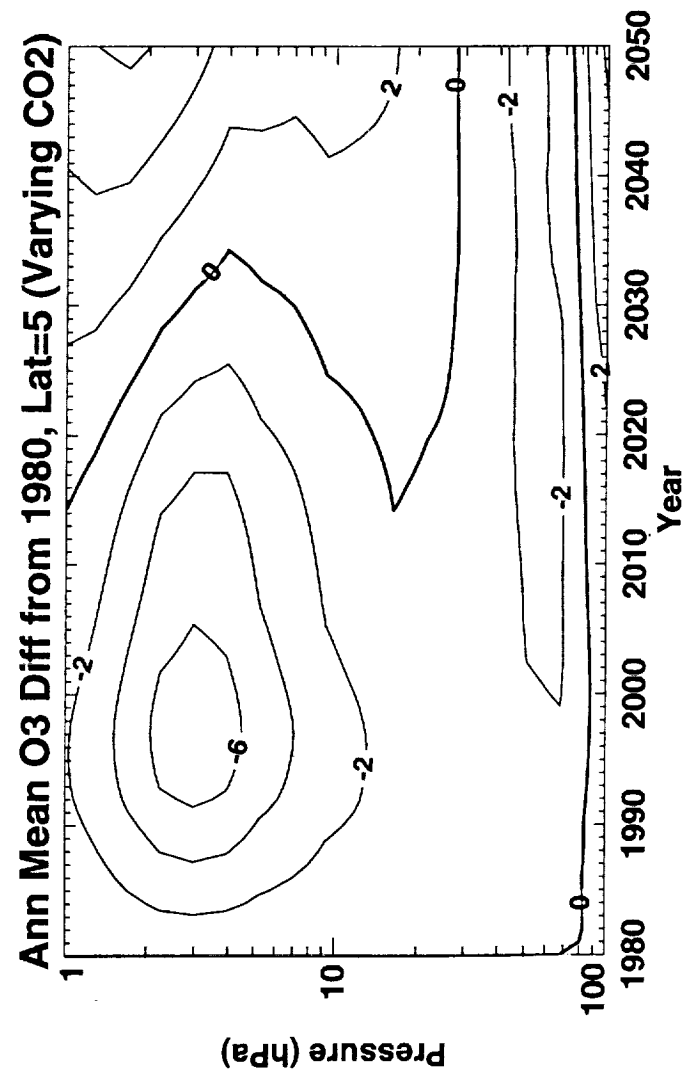
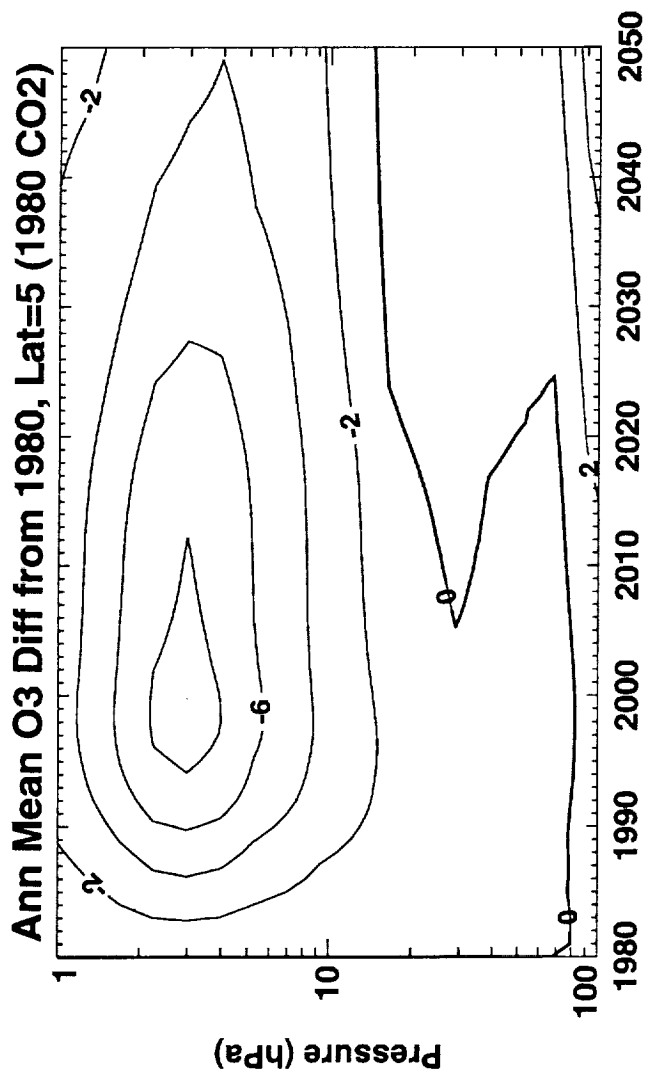


Year of Column O3 Recovery (Fixed 1980 CO2)

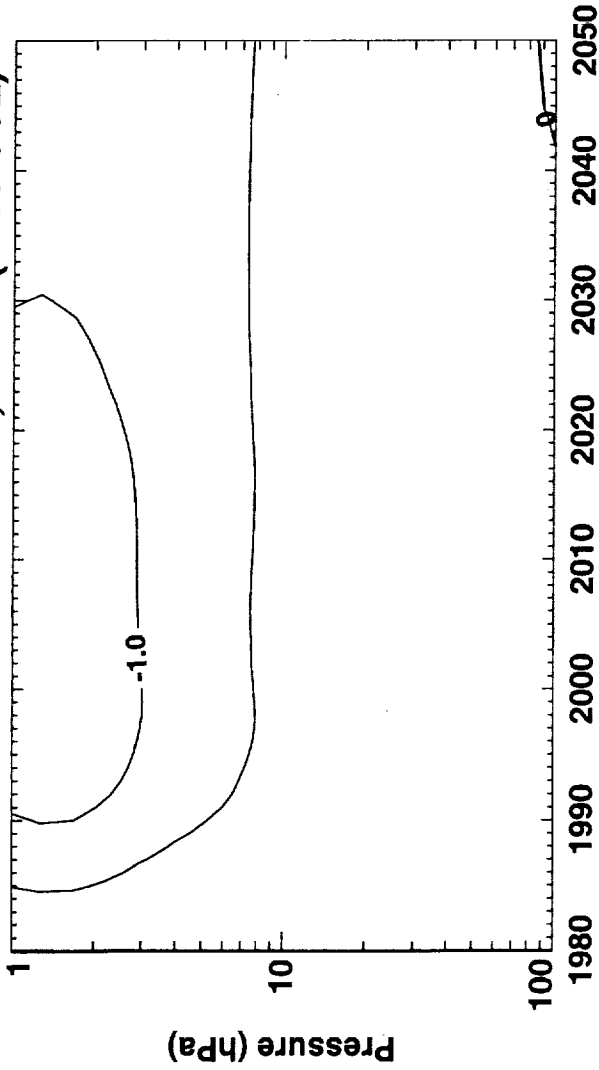


Year of Column O3 Recovery (Increasing CO2)

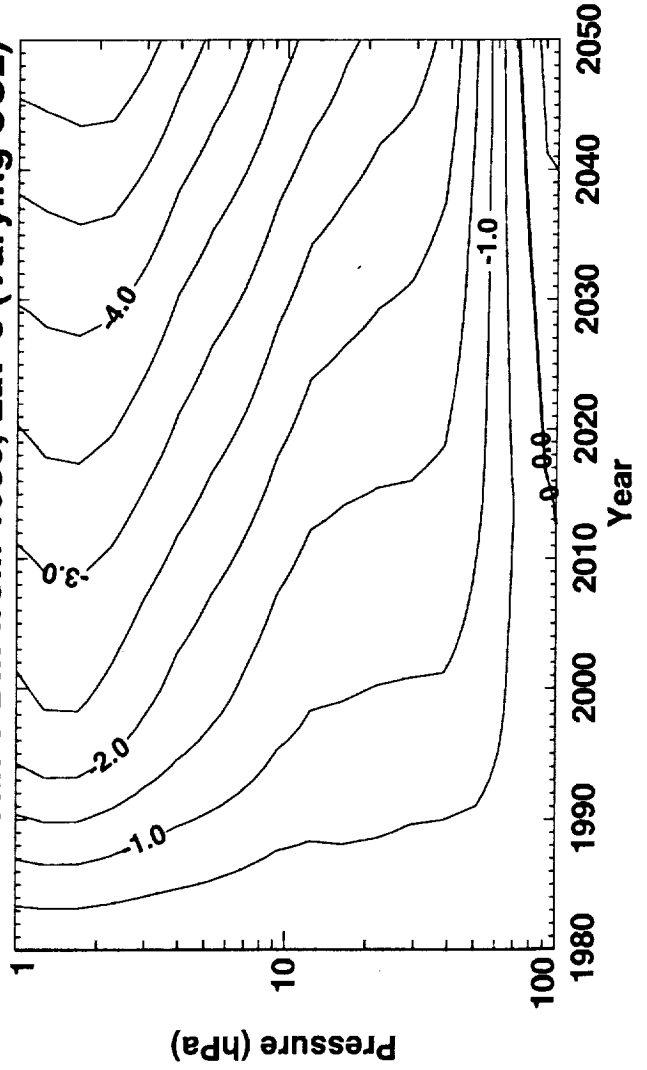


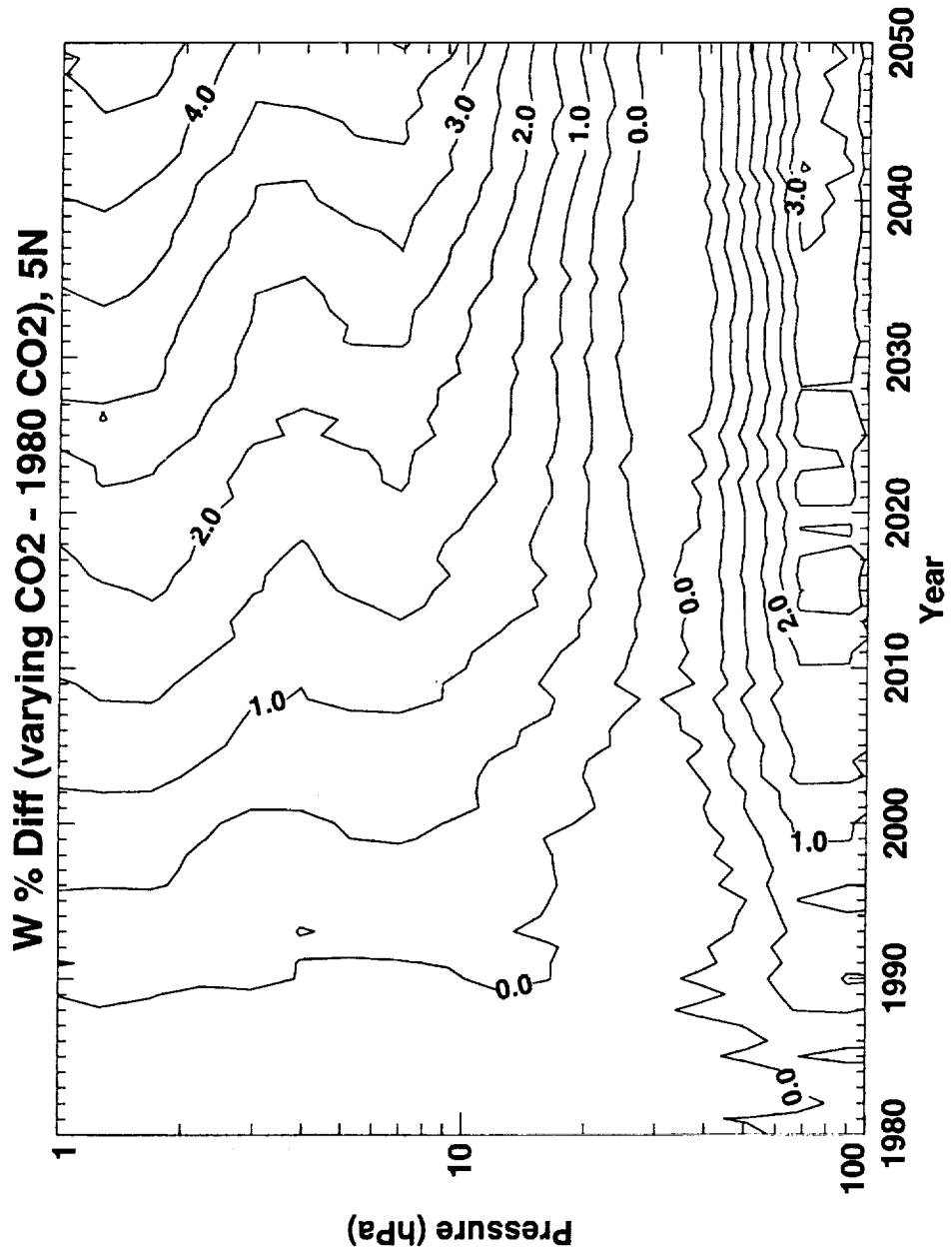


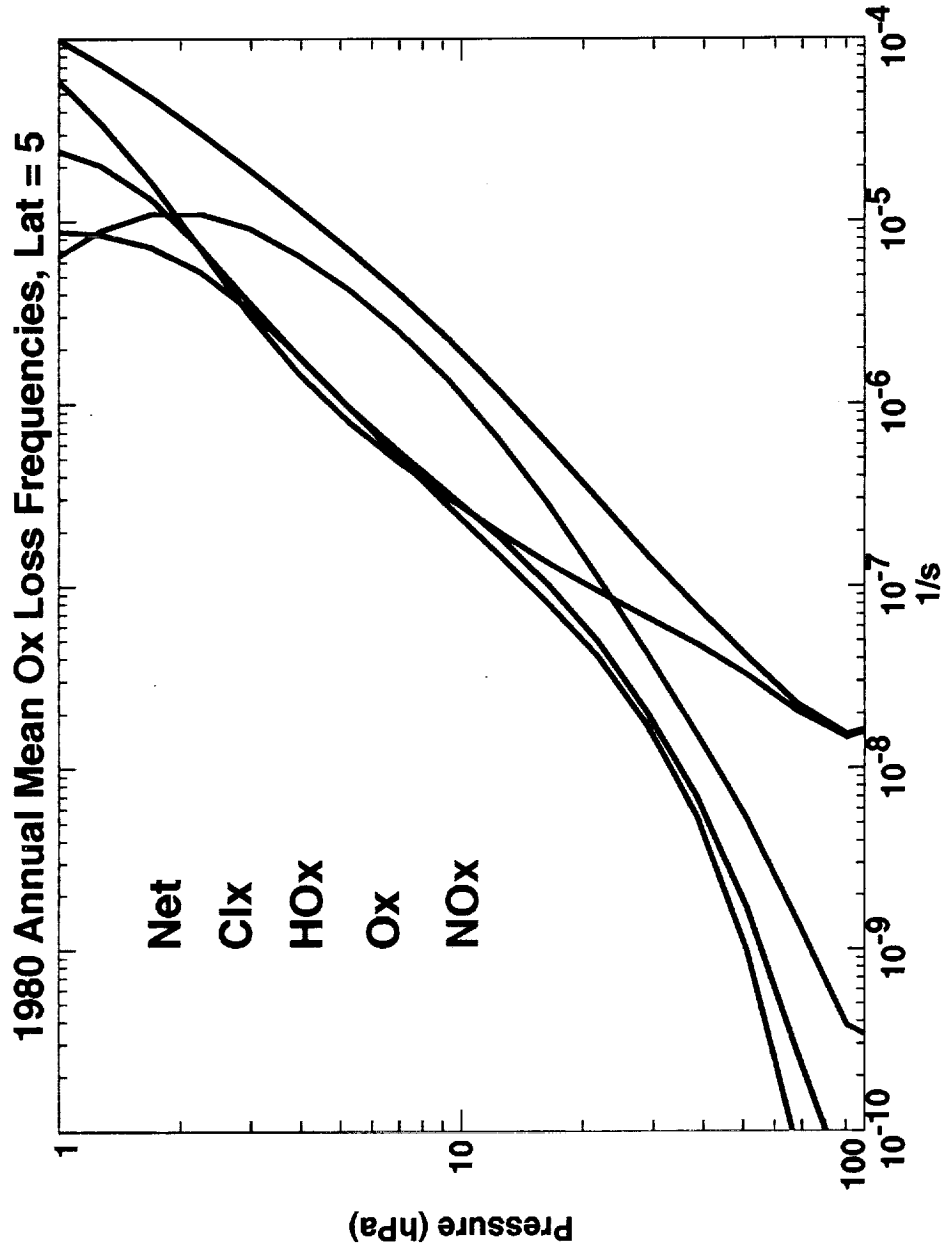
Ann Mean T Diff from 1980, Lat=5 (1980 CO2)

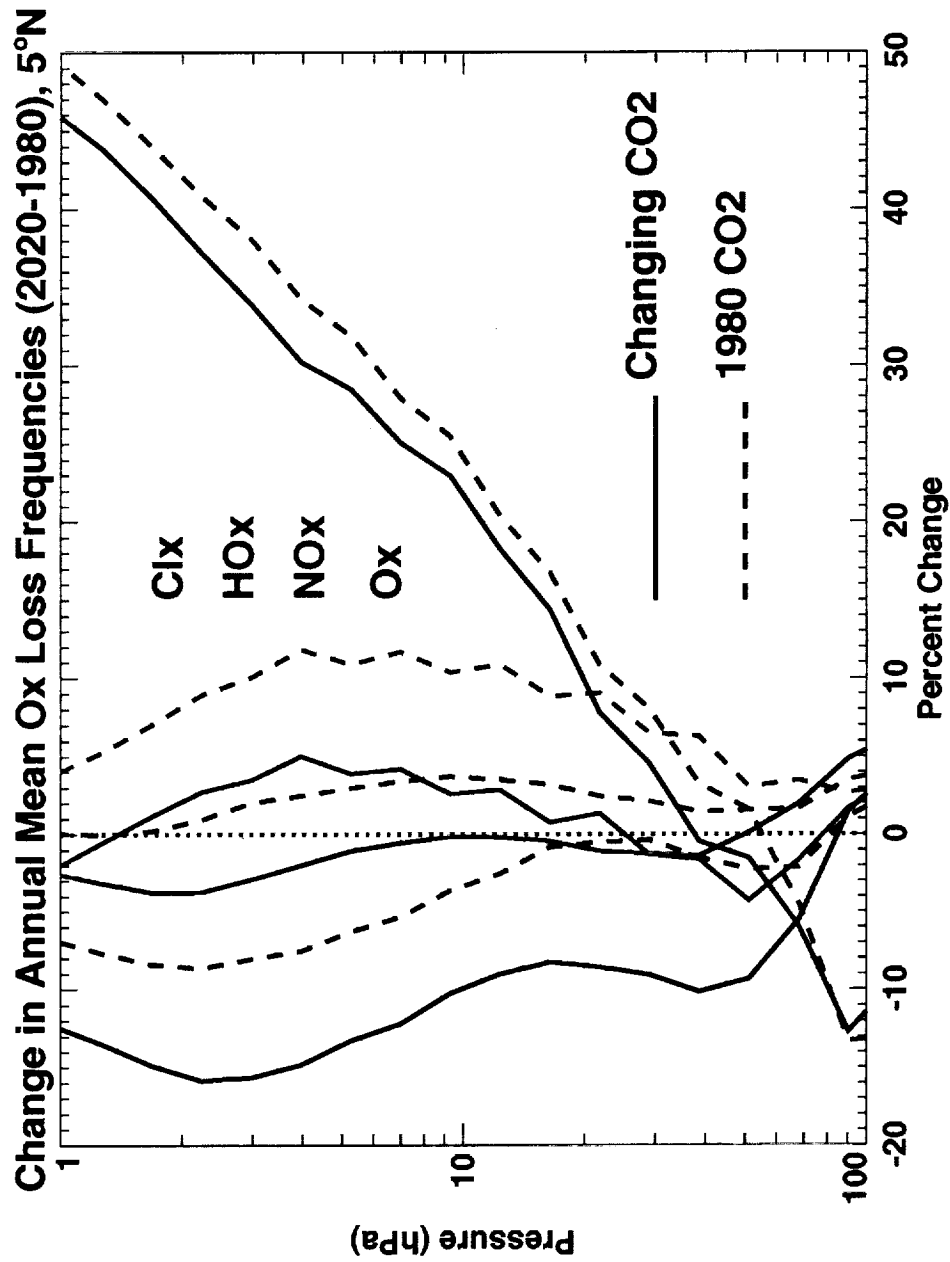


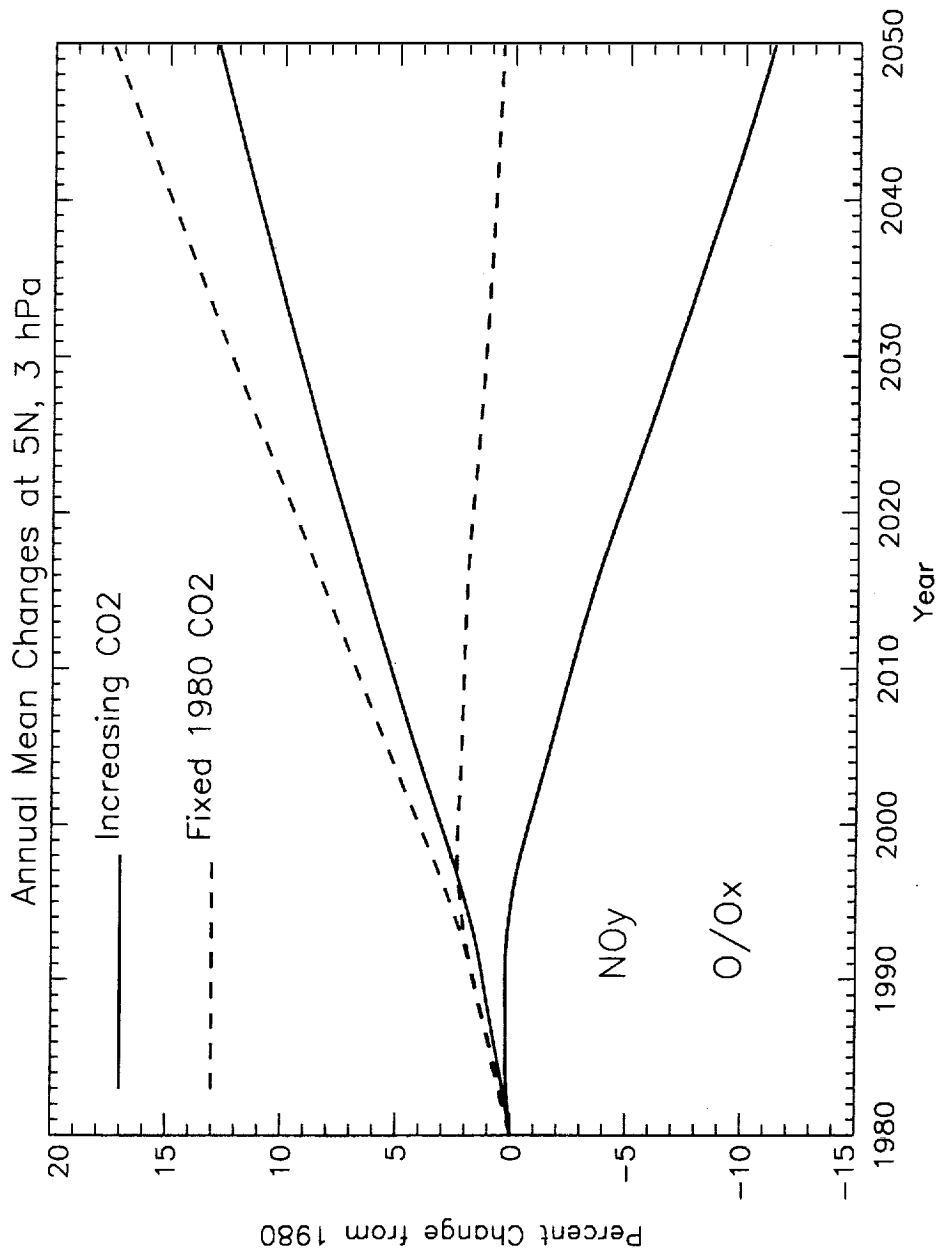
Ann Mean T Diff from 1980, Lat=5 (Varying CO2)

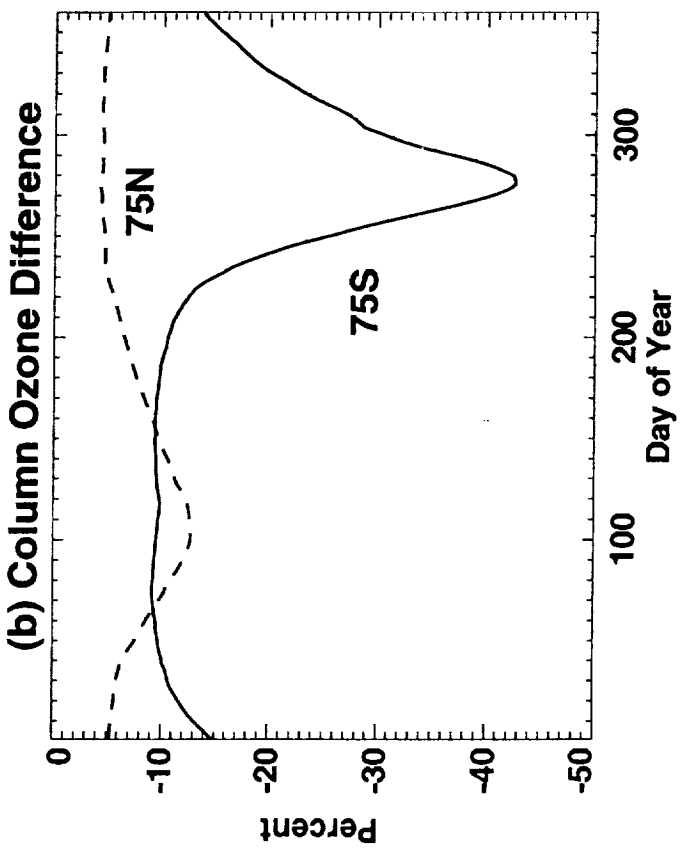
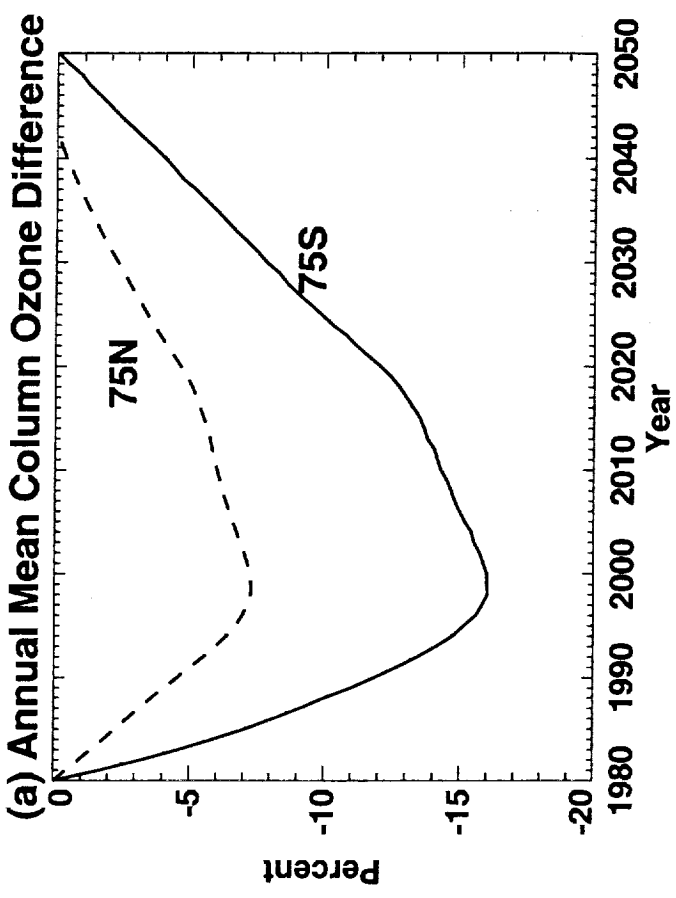


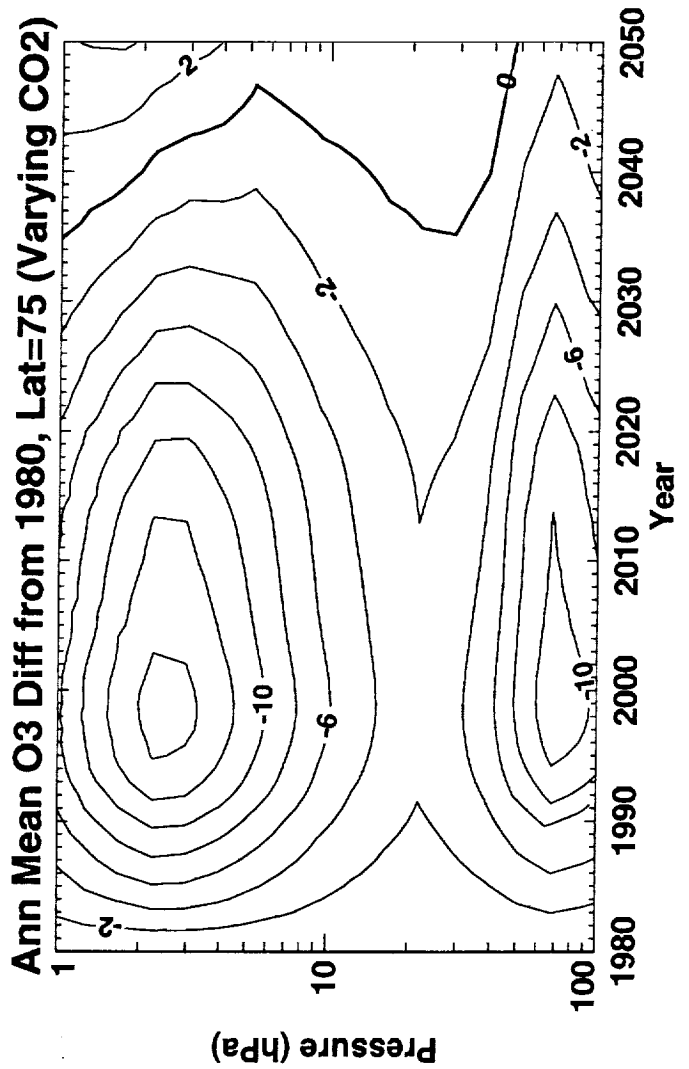
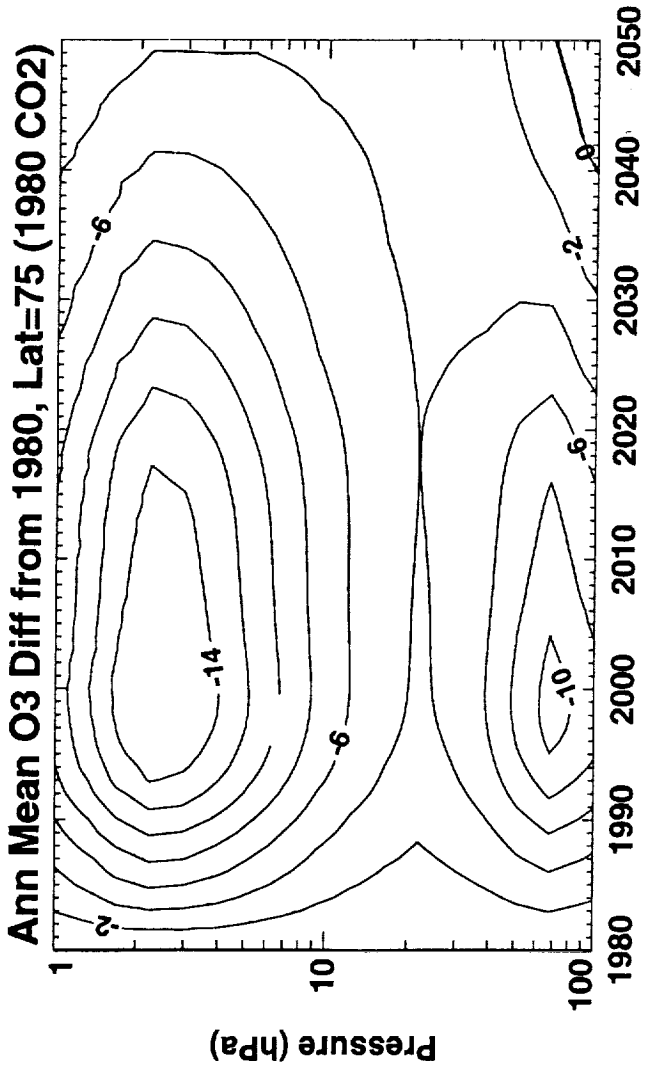


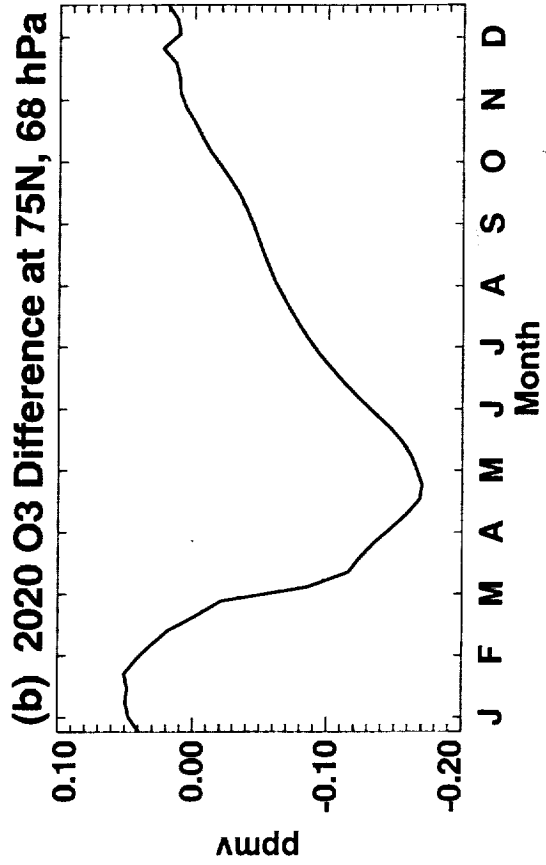
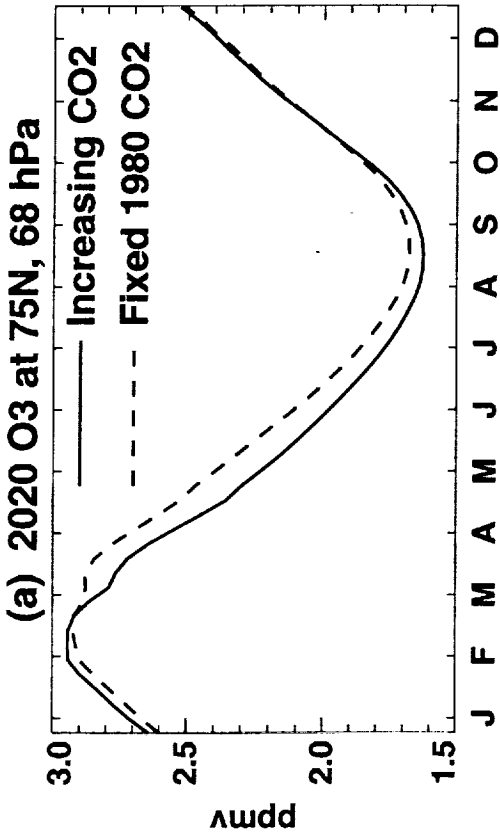




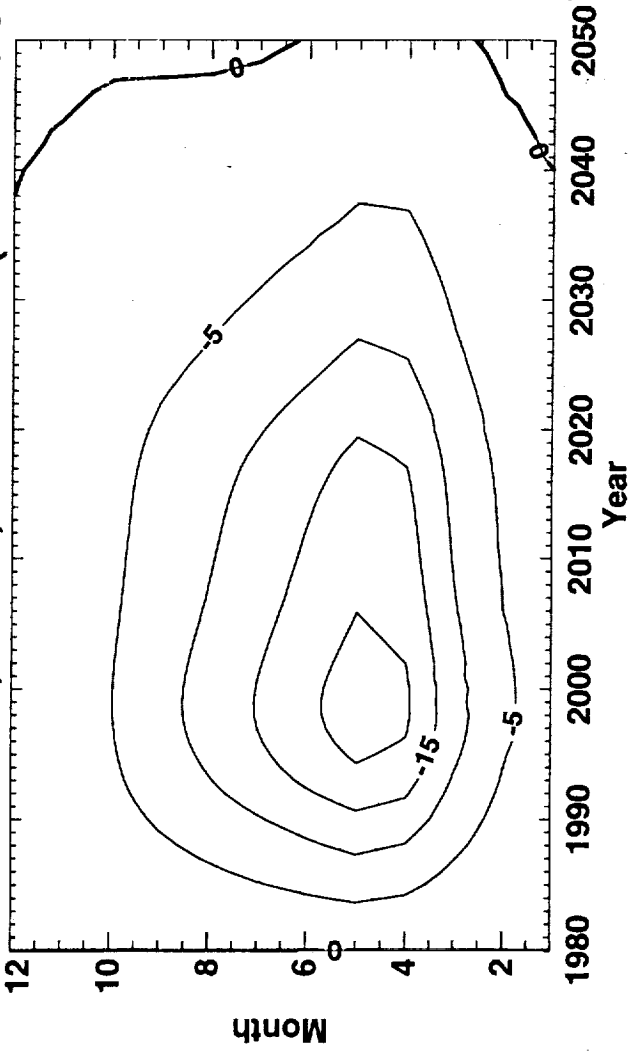








O3 % Dif from 1980, Lat=75, Pres=67 hPa (Fixed 1980 CO2)



O3 % Dif from 1980, Lat=75, Pres=67 hPa (Increasing CO2)

